

Collapse-Driven Outflow in Star-Forming Molecular Cores

Kohji Tomisaka

Faculty of Education and Human Sciences, Niigata University, 8050 Ikarashi-2, Niigata
950-2181, Japan

ABSTRACT

Dynamical collapses of magnetized molecular cloud cores are studied with magnetohydrodynamical simulations from the run-away collapse phase to the accretion phase. In the run-away collapse phase, a disk threaded by magnetic field lines is contracting due to its self-gravity and its evolution is well expressed by a self-similar solution. The central density increases greatly in a finite time scale and reaches a density at which an opaque core is formed at the center. After that, matter accretes to the newly formed core (accretion phase). In this stage, a rotationally supported disk is formed in a cloud core without magnetic fields. In contrast, the disk continues to contract in the magnetized cloud core, since the magnetic fields transfer angular momentum from the disk. Its rotation motion winds up the threading magnetic field lines. Eventually, strong toroidal magnetic fields are formed and begin to drive the outflow, even if there is no toroidal field component initially. Bipolar molecular outflows observed in protostar candidates are naturally explained by this model.

Subject headings: ISM: clouds — ISM: jets and outflows — ISM: magnetic fields — Stars: formation

1. Introduction

Star forming interstellar cores often indicate molecular bipolar outflow (for a review see Bachiller 1996). A number of driving mechanisms are proposed: a rotating disk plus threading magnetic fields (disk-driven wind model: Uchida & Shibata 1985; Pudritz & Norman 1986; Ouyed & Pudritz 1997) and interaction of stellar and disk magnetospheres (boundary layer-driven wind model: Shu et al 1994). As for the former model, when a disk with (sub-)Keplerian rotation speed is threaded by magnetic fields, it winds up the magnetic

fields and generates strong toroidal component. Resultant magnetic pressure gradient ejects matter from the disk. In contrast, Shu and collaborators (1994) proposed the interaction between stellar magnetosphere and disk magnetic field. Along the open fields where these two magnetospheres interact, disk matter is ejected by the centrifugal force.

Since rotation motion plays an important role in the dynamical contraction phase of the cloud core and thus it generates strong toroidal magnetic fields, the matter ejection seems to be driven these two. If the outflow occurs in a process of the dynamical contraction of the magnetized cloud core, it is necessary to investigate the process of gravitational contraction and outflow as a whole. However, the previous works only considered steady states or short-range time evolutions of these phenomena. Thus, in this Letter, we investigate the possibility of outflow driven by the self-gravitational contraction using ‘nested-grid’ MHD simulations.

Analytic (Larson 1969; Penston 1969; Hunter 1977; Whitworth & Summers 1985) and numerical studies (Foster & Chevalier 1993) have revealed that the dynamical collapse of a non-magnetic isothermal cloud is divided into two phases: the former “run-away collapse” phase and the latter “accretion” phase. In the former phase, the cloud shows non-homologous contraction and the central density increases greatly in a finite time scale, while in the latter accretion phase the infalling gas accretes onto a central high-density body formed in the run-away collapse phase. The latter phase corresponds to the “inside-out collapse” (Shu 1977) which is realized when accretion begins at the center of a hydrostatic cloud core. For rotating (non-magnetic) clouds (Norman, Wilson, & Barton 1980; Narita, Hayashi, & Miyama 1984) and magnetized (non-rotating) clouds (Scott & Black 1980; for recent progress, see Tomisaka 1995), these two phases exist.

The centrifugal wind model by Blandford & Payne (1982) predicts that cold disk matter could be accelerated by sufficiently strong magnetic fields when the angle between the field lines and the disk is smaller than 60° . The structure of the cloud undergoing the run-away collapse is well described with a self-similar solution and the angle is predicted as 45° with assuming that a disk is thin and the magnetic field is current-free outside the disk (Basu 1997; Nakamura & Hanawa 1997). Therefore, if a magnetized cloud is rotating, outflow may naturally be driven at some epoch in the self-gravitating contraction. To study the possibility, we performed a two-dimensional ideal MHD simulation assuming the cylindrical symmetry. In this Letter, we report that the outflow appears to emanate from the disk in the latter “accretion phase.”

2. Model

We begin our simulation from an infinitely long, cylindrical, rotating, isothermal cloud in hydrostatic balance, that is, the gravitational force is counterbalanced with the pressure force, the centrifugal force, and the Lorentz force. Here we assume the rotation axis coincides with the cylinder (z -)axis. As the initial state, only poloidal magnetic fields are taken into account and their strength is assumed proportional to the square root of local gas density. We add small density perturbations on it to initiate contraction. The initial hydrostatic state is represented by two parameters which characterize the structure: α (the ratio of magnetic pressure to the thermal one for poloidal field component) and Ω_0 (the angular rotation speed at the center of the cloud). Distributions of density, magnetic flux density, and rotation speed in the radial (r -)direction are taken identical with Matsumoto, Nakamura & Hanawa (1994), although we assume no toroidal magnetic field component B_ϕ initially. The size of the numerical box is chosen to agree with the wavelength of the most unstable mode of the self-gravitational instability λ_{MGR} (Matsumoto et al. 1994). Quantities are scaled with the isothermal sound speed c_s , the surface pressure (or surface density) $p_s = c_s^2 \rho_s$ and the corresponding scale-height $H = c_s / (4\pi G \rho_s)^{1/2}$. Typical values would be $c_s = 200 \text{ m s}^{-1}$, $\rho_s = 100 \text{ cm}^{-3}$, $H = 0.36 \text{ pc}$, and thus the time-scale is normalized by the free-fall time as $\tau_{\text{ff}} = (4\pi G \rho_s)^{-1/2} \simeq 1.75 \text{ Myr} (\rho_s / 100 \text{ cm}^{-3})^{-1/2}$. Using these scalings, initial radial distributions of density, magnetic fields and angular rotation speed are written as $\rho(r) = (\rho_c / \rho_s) \{1 + [\rho_c / \rho_s - 2(\Omega_0 \tau_{\text{ff}})^2] / [8(1 + \alpha)] \times (r^2 / H^2)\}^{-2} \rho_s$, $(B_z, B_r) = ([2\alpha \rho(r) / \rho_s]^{1/2}, 0) \rho_s^{1/2} c_s$ and $\Omega = \Omega_0 [\rho(r) / \rho_c]^{1/4}$. As model parameters, α , Ω_0 and central density ρ_c are chosen as $\alpha = 0.5$, $\Omega_0 = 5 / \tau_{\text{ff}}$, and $\rho_c = 100 \rho_s$.

Since the non-homologous gravitational contraction necessitates progressively finer spatial resolution, “nested grid technique” (Burger & Olinger 1984) is adopted, in which a number of grid systems with different spacings are prepared; the center of the cloud is covered with a finer grid and the global structure is traced by a coarser grid simultaneously. We use 15 levels of grids from L0 (the coarsest) to L14 (the finest). Grid spacing of L_n is chosen as a half of that of L_{n-1} and each level of grids uses 64×64 grid points. Thus, the smallest grid (L14’s) spacing is $\simeq 10^{-6}$ times smaller than λ_{MGR} . We applied periodic boundary conditions on the upper and lower boundaries and the fixed one on the outer boundary. Details of the numerical method have been described in separate papers (Tomisaka 1996a,b).

3. Results

3.1. Run-away Collapse Phase

The evolution is similar to that of magnetized cloud with no rotation (Tomisaka 1995, 1996a; Nakamura, Hanawa, & Nakano 1995). First, the cylindrical cloud breaks into prolate spheroidal fragments which is elongated along the cylinder axis (z -axis). As long as the amplitude of density perturbation is small $\delta\rho/\rho \lesssim 1$, the shape keeps essentially identical with the most unstable eigen-function of the gravitational instability. Next, gas begins to fall mainly along the magnetic field, and forms a disk perpendicular to the magnetic fields. The disk formed in a run-away collapse is far from static balance. However, the flow is controlled under the magnetic field and centrifugal force which lead to disk structure (pseudo-disk: Galli & Shu 1993). At $t = 0.5908\tau_{\text{ff}}$, at that time the central density ρ_c reaches $10^5\rho_s$, a shock wave is formed parallel to the disk (Figs.1a & 1b). It breaks into two waves at the epoch when the central density reaches $\rho_c \sim 10^6\rho_s$: an outer wave front propagates outwardly as a fast-mode MHD shock (seen near $z \sim 0.02H$) and an inner one does inwardly as a slow-mode MHD shock (seen near $z \sim 7 \times 10^{-3}H$) reaching the equator. The rotation angular speed Ω and toroidal magnetic field component B_ϕ also jump crossing the wave fronts. Fast rotation and thus strong B_ϕ are observed in a restricted region between these two fronts. Since the disk contracts in the radial direction, it has a larger Ω than outside the disk. In this configuration, magnetic fields transfers the angular momentum from the disk and redistributes it into the same magnetic flux tube (magnetic braking). However, from this numerical simulation it is shown that the angular momentum is confined into a region inside the fast-mode MHD shock fronts.

Although there exists a number of shock waves ($z \sim 0.02H$, $5 \times 10^{-3}H$, and $2 \times 10^{-4}H$) propagating in the z -direction, no such discontinuity is found in the r -direction (Figs.1c & 1d). However, a kind of modulation is seen around a power-law distribution as $\rho(z = 0, r) \propto r^{-2}$, which is related to the formation of multiple shock waves in the z -direction (this is found by Norman et al (1980) for the case of rotating isothermal cloud). The run-away collapse continues till $t \simeq 0.6\tau_{\text{ff}}$ and the central density would increase greatly if the isothermal equation of state continues to be valid. However, when the central density exceeds 10^{10}cm^{-3} , the central part of the core becomes optically thick for the thermal radiation from dusts and its temperature begins to rise (for example, Masunaga, Miyama, & Inutsuka,1998).

3.2. Accretion Phase

In the accretion phase, gas continues to accretes onto the newly formed opaque core. We mimic the situation by using a double polytrope composed of an isothermal one for low

density as $p = c_s^2 \rho$ for $\rho < \rho_{\text{crit}}$ and a harder one for high density as $p = p(\rho_{\text{crit}})(\rho/\rho_{\text{crit}})^\Gamma$ for $\rho > \rho_{\text{crit}}$. We take $\rho_{\text{crit}} = 10^8 \rho_s = 10^{10} \text{cm}^{-3} (\rho_s/100 \text{cm}^{-3})$ and $\Gamma = 5/3$. By virtue of this assumption we can follow further evolution. Figure 2a shows the structure captured by L8 just after the isothermal equation of state is broken. A disk, which runs vertically, contracts radially and gas motion drags and squeezes the magnetic field lines to the center. The rotation speed v_ϕ at that time is not more than the radial infall speed v_r which is in the range of $(2 - 3) \times c_s$ (see Fig. 1d).

In the accretion phase, the inflow speed is accelerated at least to $(4 - 5) \times c_s$ and as a result magnetic field lines are strongly dragged and squeezed to the center (see Fig.1c of Tomisaka 1996b). Beside these, the rotation speed is accelerated as the infall proceeds. Just after the state shown in Figure 1 with the highest central concentration, v_ϕ reaches $\simeq 4c_s$ at the distance of $r \sim 3 \times 10^{-4}H$ inside of which a nearly spherical core is formed supported mainly by thermal pressure. The rotation velocity v_ϕ exceeds the radial velocity v_r in the accretion phase, while v_ϕ was smaller than v_r (see Fig. 1d) in the run-away collapse phase. From this epoch, outflow from the disk is observed.

Figure 2 shows the structures before (a) and after (b) the outflow begins. The physical time scale between Figures 2a and 2b is approximately equal to $\simeq 1000 \text{yr} (\rho_s/100 \text{cm}^{-3})^{-1/2}$. The directions of the magnetic fields in the disk is much affected by the radial inflow. They are pushed and squeezed to the center. It is shown that in the seeding region of the outflow the angle between a magnetic field line and the disk plane decreases from $60^\circ - 70^\circ$ (Fig.2a) to $10^\circ - 30^\circ$ (Fig.2b). In Figure 2b, it is indicated that the outflow, which reaches $z_s \sim \pm 0.003H \simeq \pm 200 \text{AU} (H/0.36 \text{pc})$, is confined into two expanding bubbles whose centers are at $z_c \sim \pm 0.0015H$. In the bubble, the strength of toroidal component of magnetic fields B_ϕ is larger than that of the poloidal one $(B_z^2 + B_r^2)^{1/2}$. Especially at the outer boundary of the bubble $|B_\phi|$ is $(4 - 5)$ times stronger than $(B_z^2 + B_r^2)^{1/2}$ (see also the upper panel of Fig. 3). Further, the magnetic pressure is much larger than the thermal one. Outside of the bubble, inflow continues. The islands of strong toroidal magnetic fields which are formed just outside the disk push the poloidal fields and have an effect to strengthen the hourglass structure in the poloidal field (Ouyed & Pudritz 1997).

To see the seeding region of the outflow closely, we plot a close-up view captured by L10 in Figure 3. (Seeding region, from which outflow is ejected, moves outwardly with time. In the disk, the ratio of the centrifugal force to the gravity is no more than $\simeq 0.45$. It indicates this is far from centrifugal balanced state.) This figure shows that the outflow is ejected from the disk near $r \simeq 5 \times 10^{-4}H \simeq 40 \text{AU} (H/0.36 \text{pc})$, which is 5 times larger than the scale length for the critical density $\rho_{\text{cr}} = 10^{10} \text{cm}^{-3}$. Figure 3 clearly shows that (1) magnetic field lines are almost parallel to the disk surface near the disk. (2) gas inflow

in the disk is not disturbed by the outflow from the disk and continues to reach the central core which is supported by the thermal pressure. (3) outflow occurs along magnetic field lines whose inclination angle is in the range of $45^\circ - 60^\circ$. This corresponds to the region where $|B_\phi|$ is dominant over the poloidal component (upper panel).

Consider the main outflow ejected from $r \simeq 5 \times 10^{-4}H$ in Figure 3. Numerical simulations (Kudoh, Matsumoto, & Shibata 1998; Ouyed & Pudritz 1997) indicate that the ratio of Alfvén speed to the rotation speed is controlling how the matter is accelerated. Since this ratio is small as $0.3 - 1$ in the seeding region $r \sim 5 \times 10^{-4}H$, it is natural that the toroidal magnetic field is strongly amplified just outside of the disk. In this case, the magnetic pressure gradient is considered to play an important role to accelerate the gas after the Alfvén points located near $|z| \sim 10^{-4}H$. (In contrast, the matter is centrifugally driven when the ratio is large.) However, even in the present model, gas seems to escape from the disk with being driven centrifugally.

4. Discussion

Inflow and outflow rates are measured at the outer boundary of L10 numerical box as the surface integral of the mass flux density as $\int \rho \mathbf{v} \cdot \mathbf{n} dS$. The inflow rate is equal to $2.7 \times 10^2 c_s^3 / 4\pi G \simeq 4.1 \times 10^{-5} M_\odot \text{yr}^{-1} (c_s / 200 \text{m s}^{-1})^3$, which is almost constant in the accretion phase. It is worth noting that this is much larger than the standard accretion rate $12.25 c_s^3 / 4\pi G$ predicted for the singular isothermal sphere model (Shu 1977). This is due to the extra inflow velocity accelerated in the run-away collapse phase (Tomisaka 1996b). The outflow begins at $t \simeq 0.5998\tau_{\text{ff}}$ and the outflow rate increases with time. At the stage shown in Figure 3, it reaches $83 c_s^3 / 4\pi G \simeq 1.2 \times 10^{-5} M_\odot \text{yr}^{-1} (c_s / 200 \text{m s}^{-1})^3$. It is worth notice that the outflow rate attains $\simeq 1/3$ of the inflow rate. The ratio of outflowing mass to inflowing one decreases from L10 to L8.

Linear momentum outflow rate is also measured as the surface integral of the momentum flux density $\int \rho v_z^2 dS$ over the upper and lower boundaries of L10. This increases with time from the epoch of $t \simeq 0.5998\tau_{\text{ff}}$ and reaches $\simeq 330 c_s^4 / 4\pi G \simeq 10^{-5} M_\odot \text{km s}^{-1} \text{yr}^{-1} (c_s / 200 \text{m s}^{-1})^4$ at the epoch shown in Figure 3. This is not inconsistent with the momentum outflow rate observed around Class 0 low-mass YSOs from $^{12}\text{CO } J = 2 - 1$ line observation (Bontemps et al. 1996) as $3 \times 10^{-6} - 5 \times 10^{-4} M_\odot \text{km s}^{-1} \text{yr}^{-1}$. The maximum speed of outflow $(7 - 8) \times c_s$ is approximately equal to the Kepler speed of the seeding region, and it seems to be accelerated with increasing central mass and thus the Kepler speed. Therefore, the momentum outflow rate is likely to increase further.

Why does the outflow occur only in the “accretion phase”? Rotation velocity becomes dominant over the radial velocity only in the accretion phase. This is also indicated by a recent study using a self-similar solution for contracting isothermal rotating disk (Saigo & Hanawa 1998; see their moderately rotating model of $\omega = 0.3$). Further, toroidal magnetic fields develop only in the accretion phase.

This seems to come from the fact that the run-away collapse is fast and as a result the toroidal magnetic fields can not be developed by rotation. In other words, from numerical simulations, the angular rotation speed near the center $\Omega_c(t)$ is proportional to the central free-fall rate as $\Omega_c \simeq (0.2 - 0.4) \times (2\pi G \rho_c)^{1/2}$ (Matsumoto, Hanawa, & Nakamura 1997). Therefore, the angle that a gas element rotates in this free-fall time is as large as $\theta \sim \Omega_c / (2\pi G \rho_c)^{1/2} \sim 0.2 - 0.4$ radian. Since the disk rotates only at $\sim 0.2 - 0.4$ radian, it is concluded that the magnetic field can not be wound much in the run-away collapse phase.

In the accretion phase, we have found a rotating ring nearly in a hydrostatic balance for a model with no magnetic fields ($\alpha = 0$). Since the angular momentum in the disk is transferred to the outer region by the magnetic effect, a model with poloidal magnetic fields indicates a structure different from the non-magnetic disk. Magnetized disk consists of an innermost nearly hydrostatic core and a contracting rotating disk.

Blandford and Payne (1982) have revealed that a cold gas which rotates in a Kepler disk can escape from the stellar gravity by the effect of magnetic fields. The condition to escape is that the angle between the magnetic field lines and the disk is smaller than 60° , below which the magnetic field line can transfer enough angular momentum to the gas element to escape from the gravity of the central point mass. Although this is valid for the point mass, the angle seems to play an important role for the outflow phenomenon. Decrease in the angle is mainly due to the disk accretion (inflow) and drag. Therefore, it is concluded that the outflow is driven by a rotating contracting cloud core only in the accretion phase.

I would like to thank Dr. F. Nakamura for careful reading the manuscript and Dr. R. Pudritz, referee, for his comments to improve the paper. Numerical simulations were performed by Fujitsu VPP300/16R supercomputer at the Astronomical Data Analysis Center of the National Astronomical Observatory, Japan.

REFERENCES

Bachiller, R. 1996, *ARA&A*, 34, 111

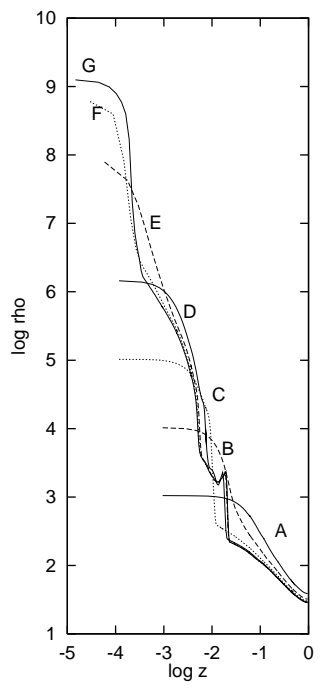
- Basu, S. 1997, *ApJ*, 485, 240
- Bontemps, S., André, P., Terebey, S., & Cabrit, S. 1996, *A&A*, 311, 858
- Burger, M.J., & Olinger, J. 1984, *J. Comput. Phys.*, 53, 484
- Blandford, R. D., & Payne, D. G. 1982, *MNRAS*, 199, 883
- Foster, P. N., & Chevalier, R. A. 1993, *ApJ*, 416, 303
- Galli, D., & Shu, F.H. 1993, *ApJ*, 417, 243
- Hunter, C. 1977, *ApJ*, 218, 834
- Kudoh, T., Matsumoto, R., & Shibata, K. 1998, submitted to *ApJ*
- Larson, R. B. 1969, *MNRAS*, 145, 271
- Masunaga, H., Miyama, S. M., & Inutsuka, S. 1998, *ApJ*, 495, 346
- Matsumoto, T., Hanawa, T., & Nakamura, F. 1997, *ApJ*, 478, 569
- Matsumoto, T., Nakamura, F., & Hanawa, T. 1994, *PASJ*, 46, 243
- Nakamura, F., & Hanawa, T. 1997, *ApJ*, 480, 701
- Nakamura, F., Hanawa, T., & Nakano, T. 1995, *ApJ*, 444, 770
- Narita, S., Hayashi, C., & Miyama, S. M. 1984, *Prog. Theor. Phys.*, 72, 1118
- Norman, M. L., Wilson, J. R., & Barton, R. T. 1980, *ApJ*, 239, 968
- Ouyed, R., & Pudritz, R. E. 1997, *ApJ*, 484, 794
- Penston, M. V. 1969, *MNRAS*, 144, 425
- Pudritz, R. E., & Norman, C. A. 1986, *ApJ*, 301, 571
- Saigo, K., & Hanawa, T. 1998, *ApJ*, 493, 342
- Scott, E. H., & Black, D. C. 1980, *ApJ*, 239, 166
- Shu, F. H. 1977, *ApJ*, 214, 488
- Shu, F. H., Najita, J., Ostriker, E., Wilkin, F., Ruden, S., & Lizano, S. 1994, *ApJ*, 429, 781
- Tomisaka, K. 1995, *ApJ*, 438, 226
- Tomisaka, K. 1996a, *PASJ*, 48, 701
- Tomisaka, K. 1996b, *PASJ*, 48, L97
- Uchida, Y., & Shibata, K. 1985, *PASJ*, 37, 515
- Whitworth, A., & Summers, D. 1985, *MNRAS*, 214, 1

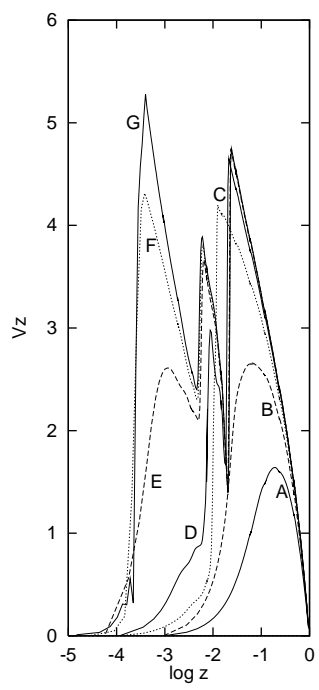
Figure Captions

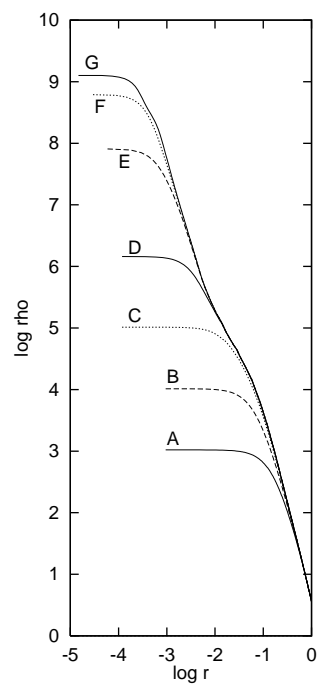
Fig. 1.— Distributions of the density and infall speed along the z -axis are plotted in (a) $\log \rho(z, r = 0)$ and (b) $|v_z(z, r = 0)|$ respectively. Those along the equatorial plane are also shown in (c) $\log \rho(z = 0, r)$ and (d) $|v_r(z = 0, r)|$. Snapshots are made at $t = 0.5233\tau_{\text{ff}}$ ($\rho_c \sim 10^3 \rho_s$ A), $t = 0.5725\tau_{\text{ff}}$ ($\rho_c \sim 10^4 \rho_s$ B), $t = 0.5908\tau_{\text{ff}}$ ($\rho_c \sim 10^5 \rho_s$ C), $t = 0.5977\tau_{\text{ff}}$ ($\rho_c \sim 10^6 \rho_s$ D), $t = 0.5994\tau_{\text{ff}}$ ($\rho_c \sim 10^8 \rho_s$ E), $t = 0.5996\tau_{\text{ff}}$ ($\rho_c \sim 10^{8.8} \rho_s$ F), and $t = 0.5997\tau_{\text{ff}}$ ($\rho_c \sim 10^{9.1} \rho_s$ G). Rotation velocity distribution along the equatorial plane is plotted for the epoch G in (d).

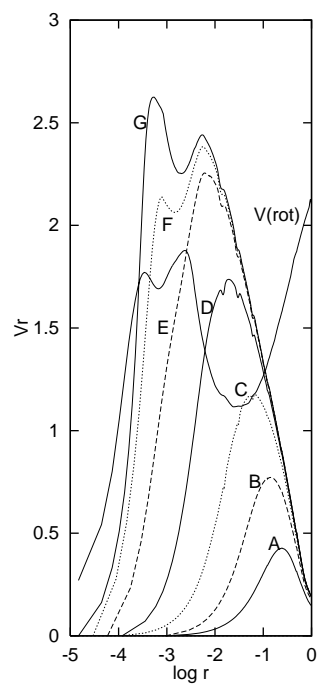
Fig. 2.— Left: isodensity lines, magnetic field lines, and velocity vectors are plotted for the state when the central density reaches $10^{8.8} \rho_s$ ($t = 0.5996\tau_{\text{ff}}$). In contrast to the usual usage, the z -axis is placed horizontally and the r -axis is vertically. Right: the same as (a) but for the state when the central density reaches $10^{10} \rho_s$ ($t = 0.6002\tau_{\text{ff}}$). Both are Level 8. Physical time passed between these two is equal to $1000 \text{ yr } (\rho_s/100\text{cm}^{-3})^{-1/2}$.

Fig. 3.— Close-up view of the seeding region of the outflow. False colors represent the ratio of the toroidal magnetic pressure $B_\phi^2/8\pi$ to the poloidal one $(B_z^2 + B_r^2)/8\pi$ in the upper panel and the density distribution ρ in the lower panel, respectively. Velocity vectors (v_z, v_r) and magnetic field lines (B_z, B_r) are also plotted. This figure shows Level 10 which has 4-times finer spatial resolutions than the previous one ($-10^{-3}H \leq z \leq 10^{-3}H$ and $0 \leq r \leq 2 \times 10^{-3}H$).









This figure "fig2a.gif" is available in "gif" format from:

<http://arxiv.org/ps/astro-ph/9806085v1>

This figure "fig2b.gif" is available in "gif" format from:

<http://arxiv.org/ps/astro-ph/9806085v1>

This figure "fig3.gif" is available in "gif" format from:

<http://arxiv.org/ps/astro-ph/9806085v1>